1998

Origin and evolution of the Cepheus bubble

NA Patel

PF Goldsmith

MH Heyer

RL Snell

P Pratap

THE ASTROPHYSICAL JOURNAL, 507:241–253, 1998 November 1

ORIGIN AND EVOLUTION OF THE CEPHEUS BUBBLE

NIMESH A. PATEL
Smithsonian Astrophysical Observatory, 60 Garden Street, Cambridge, MA 02138; npatel@cfa.harvard.edu
PAUL F. GOLDSMITH
National Astronomy and Ionospheric Center, Cornell University, NAIC, Department of Astronomy, Ithaca, NY 14853
MARK H. HEYER AND RONALD L. SNELL
Five College Radio Astronomy Observatory, University of Massachusetts, Amherst, MA 01003
AND
PREETHI PRATAP
Haystack Observatory, Westford, MA 01886-1299
Received 1997 December 10; accepted 1998 June 10

ABSTRACT

We have imaged a $10^\circ \times 10^\circ$ region of the Cepheus bubble in the $J = 1$–0 line of CO and the 21 cm line of atomic hydrogen. The CO emission defines a giant expanding shell 120 pc in diameter, which is similar to that seen in the *IRAS* sky maps. We estimate the total gas mass in the region to be $\sim 4 \times 10^5$ $M_\odot$. The total kinetic energy from the observed spread of velocities of the molecular clouds is $\sim 10^{51}$ ergs. We suggest that the members of earlier generations of massive stars in NGC 7160 are responsible for the origin of the Cepheus bubble. These stars created an expanding compressed shell of gas that became gravitationally unstable at an age of ~ 7 Myr. The members of the Cepheus OB2 association comprise the second, intermediate generation of stars in this region that formed as a consequence of this instability. The numerous color selected *IRAS* point sources represent the third and youngest generation of stars in this region. Our observations suggest the great importance of sequentially triggered star formation in the region of the Cepheus bubble.

Subject headings: ISM: bubbles — ISM: individual (Cepheus bubble) — ISM: molecules — open clusters and associations: individual (Cepheus OB2) — radio lines: ISM

1. INTRODUCTION

The Cepheus bubble is a giant shell with a diameter of about 10° (~ 120 pc, based on a distance of ~ 800 pc; Ábráham et al. 1993) appearing on the *IRAS* 60 and 100 μm sky flux maps centered at $l \sim 102\overset{\circ}{.}5$ and $b \sim 6\overset{\circ}{.}5$. This ring of infrared emission was discovered by Kun, Balázs, & Toth (1987). A similar structure appears in the older photographic atlases of H II regions made in Hα emission by Sivan (1974) and Dubout-Crillon (1976), which show the bubble as an outline traced by the Sharpless H II regions including IC 1396 (S131) and S140.

H I mapping of the Cepheus bubble region was carried out by Simonson & van Someren Greve (1976). Large-scale ^{13}CO maps in the Cygnus region, which also include the Cepheus bubble region, have been presented by Dobashi et al. (1994). In both these studies, the poor angular resolution and sampling make comparison with the infrared image of the bubble difficult.

Expanding shells of dense gas around H II regions have been inferred in several previous studies of CO emission from the molecular clouds around OB stars such as the clouds around λ Orionis (Maddalena & Morris 1980), Gemini OB1 (Carpenter, Snell, & Schloerb 1995), Monoceros R2 (Xie & Goldsmith 1994), the Gum Nebula (Sridharan 1992), and W33 (Keto & Ho 1989), to note a few examples. To improve our understanding of how UV radiation and stellar winds from young massive stars affect the structure and evolution of molecular clouds, it is important to map these objects at high angular resolution without compromising on sampling. Images of molecular gas often reveal rings and cavities presumably blown by the stellar winds and/or photoionizing radiation from early-type stars (Patel et al. 1995; Carpenter et al. 1995; Xie & Goldsmith 1994). The compression of the gas in such regions may lead to further star formation (Elmegreen 1992 and references therein). We previously carried out a comprehensive study of the bright rimmed globules associated with the H II region IC 1396 (Patel et al. 1995). This study explored the idea of star formation initiated by radiative implosion of bright rimmed globules and the acceleration of the globules by the photoionizing radiation from the exciting O-type star powering the H II region. The globules of IC 1396 appear to be located on a localized expanding ring. The origin of this ring can be understood as a consequence of secondary expansion due to photoionization effects in a preexisting compressed spherical shell of dense gas from which the O-type star HD 206267 formed. The existence of such a spherical shell was suggested by the *IRAS* maps (see Figs. 13 & 14 of Patel et al. 1995).

In this paper, we present a much larger set of CO data, covering the entire region occupied by the Cepheus bubble, and investigate further some of these ideas. Our goal is to achieve a better understanding of the phenomena associated with the interaction between young massive stars and the surrounding interstellar medium and, specifically, the process of triggered star formation. By studying the morphology and association of the CO emission relative to the distribution of young massive stars, and with *IRAS* point sources indicating embedded young stellar objects, we attempt to understand the origin and evolution of the Cepheus bubble. We also present the kinematics of the molecular clouds associated with the Cepheus bubble as revealed by the CO spectra. We present the details of our observations in the following section and in § 3 present the

results. In § 4 we discuss and interpret the results and in § 5 summarize our conclusions.

2. OBSERVATIONS

The observations reported in this paper consist primarily of CO 1–0 mapping of a 72° square region in Cepheus selected according to the *IRAS* 100 μm emission map. The sampling in the map was 50″ with an FWHM resolution of 45″. Approximately 387,000 spectra were obtained between 1993 December and 1994 March using the FCRAO 14 m telescope at New Salem, Massachusetts. This was one of the relatively early projects employing the focal plane array receiver QUARRY (Erickson et al. 1992), and hence the back-end spectrometers available were less than ideal. We used two filter banks having resolutions of 1 MHz per channel and 250 KHz per channel, each with 32 channels per QUARRY pixel. The latter filter bank did not offer adequate velocity coverage for the entire region that was mapped, and these data were not included in the present paper. The 1 MHz per channel filter bank provided a velocity coverage of about 100 km s^{-1} centered on $V_{\rm LSR} = -10$ km s^{-1}.

Observations were made in position-switching mode, with the reference position bootstrapped as the mapping proceeded, to select an area free of CO emission. The fiducial position of the map $(\Delta\alpha, \Delta\delta) = (0', 0')$ is at $\alpha(1950) = 21^{\rm h}18^{\rm m}00^{\rm s}$, $\delta(1950) = 59°30'00''$, near S129. The reference position was typically 1°–2° away from the main position. Integration time was between 20 and 30 s per pointing, resulting in an rms noise of 0.1–0.2 K. Pointing was checked repeatedly on planets and the SiO maser source T Cephei. Pointing and gain calibration were also checked periodically by observing the edge of globule A in IC 1396. The rms pointing error was found to be about 5″. The main beam efficiency at 115 GHz is about 0.45 with a small elevation dependence that is neglected here. Portions of the image included data taken previously by Heyer, Carpenter, & Ladd (1996) and Patel et al. (1995). The southeastern periphery of our Cepheus bubble map also overlaps with the subsequent CO mapping of the FCRAO CO survey of the outer galaxy (Heyer et al. 1997).

The Cepheus bubble region was also observed in the 21 cm hyperfine transition of atomic hydrogen using the Dominion Radio Astronomical Observatory 26 m single dish antenna. We obtained a 48 × 48 point (12° × 12°) Nyquist-sampled map of the region almost exactly covering our CO map of the Cepheus bubble. The angular resolution is 31′ with sampling every 16′, and the velocity resolution is 0.82 km s^{-1} (128 channels centered on $V_{\rm LSR} = -10$ km s^{-1}).

3. RESULTS

Figure 1 is a map of the peak emission intensity showing the maximum antenna temperature of the CO 1–0 line. The CO emission extends between −20 and 9 km s^{-1} $V_{\rm LSR}$. The integrated intensity in this velocity range is similar to the peak intensity map, implying that the intrinsic line width of the CO emission does not vary significantly across the region. Variations in the line shape would not likely be revealed by our coarse frequency resolution of 1 MHz, so the present work is unable to address any questions that depend upon the line profiles of the CO emission. The peak intensity image thus represents the integrated intensity image within an overall multiplicative factor that we assume to be constant throughout the image. From the underresolved CO spectra in certain regions, we can still obtain reliable information on the overall kinematics of the clouds associated with the Cepheus bubble.

The CO antenna temperature is at its maximum in the clouds associated with S140, where it reaches a value of 10 K. However, most features in Figure 1 that are distributed in filaments or globules show values of antenna temperature typically between 2 and 8 K, whereas the diffuse clouds are significantly fainter.

There are several new clouds that have not been previously identified either by visual extinction (Lynds catalog) or by the lower angular resolution and sampling in existing CO surveys (e.g., Dame et al. 1987; Dobashi et al. 1995; Leisawitz, Bash, & Thasseus 1989). The filamentary appearance of clouds tends to conform to the overall ringlike geometry as seen in Figure 1. Some of the filaments appear to form secondary rings much like the IC 1396 system of globules, including the ones near L1204 (420′, 100′), S134 (400′, −60′), and S129 (0′, 0′). The relatively strong CO emission seen at the very north end of our map traces the region around NGC 7129 that is unlikely to be associated with the Cepheus bubble. There is another ringlike structure centered at (−20′, 200′).

The total velocity range over which we detect CO emission extends from −27.5 to +8.5 km s^{-1} $V_{\rm LSR}$. In IC 1396 we assumed a systemic velocity of $V_{\rm LSR} = -2$ km s^{-1} (Patel et al. 1995) based on the H166α line observations made by Pedlar (1980). If we assume this as our reference velocity representing the velocity of the ionized gas in the interior of the bubble to be the same, then the CO emission appearing on the channel maps in Figure 2 can be considered in the following fashion. Panels 1–6 represent the extremely blueshifted velocities, panels 7 and 8 represent the moderately blueshifted gas, and panel 9 represents the "rest" velocity gas, while the redshifted material is shown in panels 10 and 11. Panel 12 shows the extremely redshifted emission at the southwest edge of the map that is most likely unrelated to the bubble. Note that the blueshifted gas appears near the lower left (southeast) corner of the map (panels 1 and 2), and the most redshifted gas appears in panel 11, at the northwest end of the map. This velocity gradient is perpendicular to the galactic plane, with the blueshifted gas closer to and the redshifted gas farther from the plane.

3.1. *Cepheus OB2 and Surrounding* H II *Regions*

To relate the distribution of young massive stars to that of the molecular clouds in the Cepheus bubble region, we selected stars in the range of spectral types between O and B2 from the Position and Proper Motions Catalog (Roeser & Bastian 1988) and found 49 stars, including six O-type stars. The spectral types and coordinates were cross-compared with the SAO J2000 catalog and with previous compilations of OB stars by Cruz-Gonzalez et al. (1974), Humphreys (1978), Simonson (1968), Karimova & Pavlovskaya (1981), Gies (1987), Garmany, Conti, & Chiosi (1982), and Stone (1979). Table 1 lists these OB stars. The search was carried out in the region shown in Figure 3 extending beyond the boundaries of our CO map. In this figure, the large symbols indicate O-type stars and small symbols indicate B0–B2-type stars. The vacuous regions on the CO map are coincident with largest concentration of young massive stars, suggesting that most of the gas in these regions is ionized. The circles indicate only the sizes of Sharpless H II

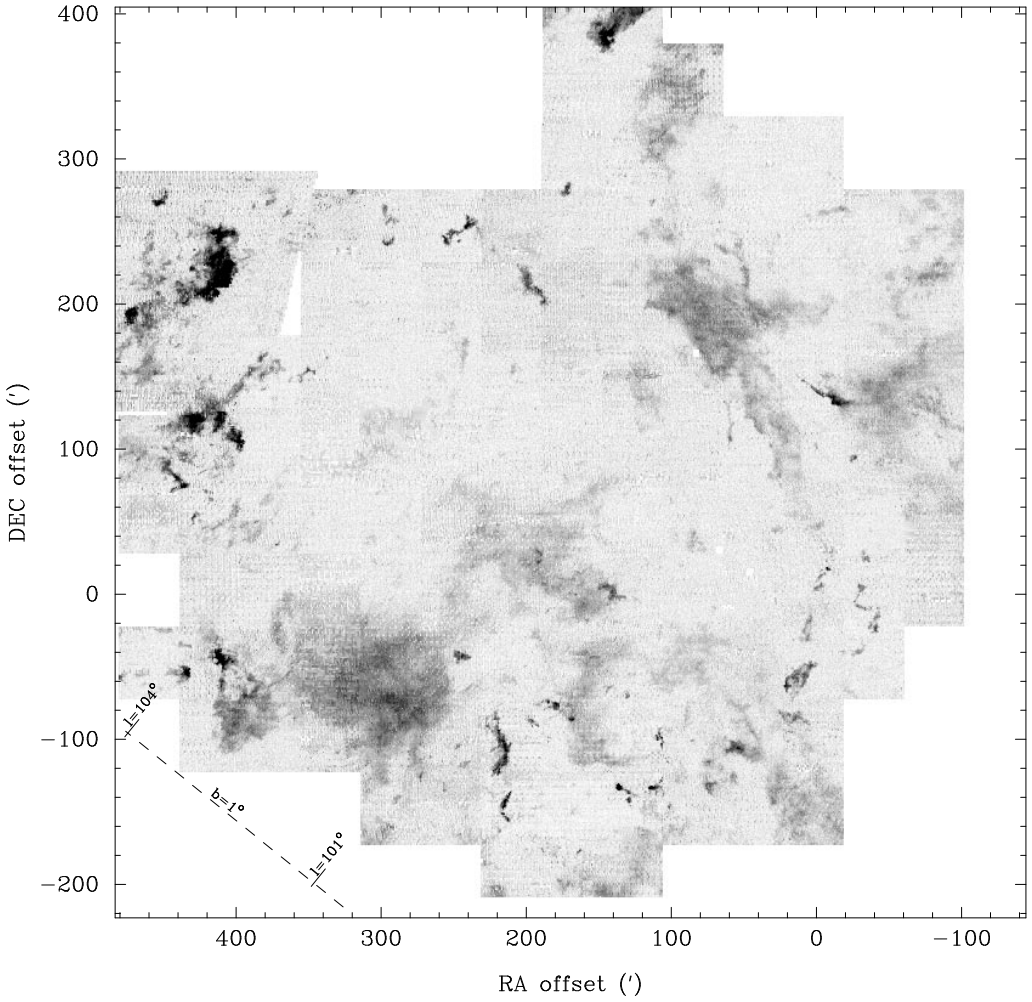

FIG. 1.—Peak intensity of CO 1–0 emission. The gray scale represents antenna temperature values scaled linearly between 0 and 3.5 K. The strongest emission occurs at the S140 region and globule A of IC 1396, where the peak antenna temperature is about 10 K. The position offsets are measured from $\alpha(1950) = 21^{h}18^{m}00^{s}$, $\delta(1950) = 59°30'00''$, near S129.

regions (Sharpless 1959) and not necessarily their morphology. For example, S133 is a partial arc of ionized emission (Ábráham et al. 1993). These H II regions highlight the circular arrangement along the periphery of the bubble. The O stars themselves form a smaller ring that lies within the larger ring defined by CO and the infrared emission (Kun et al. 1987). The region of Cepheus bubble includes the Cepheus OB2 (CepOB2) association (also known as Cepheus II and I Cephei), which, in part, is made up of clusters Trumpler 37 and NGC 7160. These two subgroups are separated by 80 pc and are moving away from each other at a speed of 20 km s^{-1}, corresponding to an expansion age of 4 Myr (Blaauw 1964). The age of the older group NGC 7160 and of the group of evolved stars in the region of CepOB2 is between 10 and 18 Myr (Conti & van den Heuvel 1970; Simonson & van Someren Greve 1976; Janes & Adler 1982). According to Blaauw (1961), the runaway stars λ Cep and 68 Cyg have originated from this region, indicating that at least one supernova has exploded there.

3.2. *IRAS Point Sources: Present Star Formation*

As a first step in identifying the "third" generation of stars that is currently forming in the molecular clouds in the Cepheus bubble region, we have selected *IRAS* points sources according to their *IRAS* color criteria as suggested by Beichman, Boulanger, & Moshir (1992) to represent young stellar objects as in our previous work on IC 1396 (Patel et al. 1995). Figure 4 shows the location of these sources with respect to the CO emission. A similar search (based on less restrictive criteria) was made by Kun et al. (1987), from whose work the circular arrangement of the *IRAS* sources was clear even without considering the morphology of the molecular gas (which was then not known). It is interesting to note that the detailed correspondence between the *IRAS* sources and the molecular gas is often highly variable; there are some clouds with no *IRAS* sources, while there are *IRAS* sources present where the CO emission is below our detection limit of about 0.2 K antenna temperature.

3.3. *Mass Estimates*

The molecular gas mass based only on the CO 1–0 line has significant uncertainties because of the fact that this line is usually optically thick in molecular clouds. In order to obtain a rough estimate of the masses of the molecular clouds associated with the Cepheus bubble, we simply use the integrated CO emission, $\int T_A\,dV$, and a conversion factor between the molecular hydrogen column density, N_{H_2}, and the integrated CO emission equal to 2.3×10^{20} cm^{-2}(K km $s^{-1})^{-1}$ (e.g., Rolfs & Wilson 1996). We obtain a

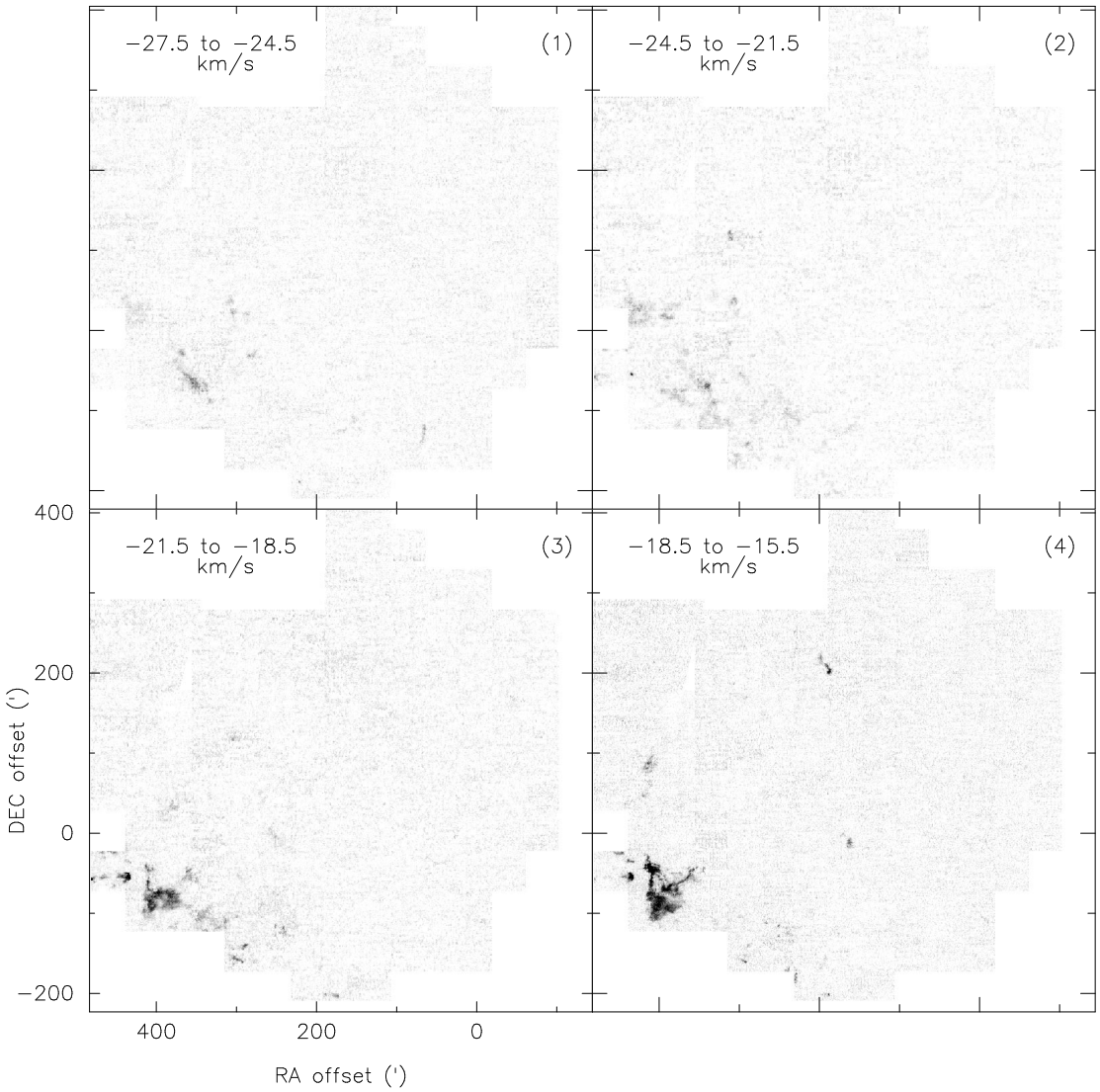

FIG. 2.—Velocity channel maps of the CO 1–0 emission. The emission appearing in the 5.5–8.5 km s^{-1} interval is probably not associated with the Cepheus bubble.

value of $5 \times 10^4\ M_\odot$ for the molecular gas mass. In the regions that were mapped previously in ^{13}CO with the same instrument (IC 1396, Patel et al. 1995; S140, Heyer et al. 1996), we have a somewhat better estimate of molecular gas mass. We used these data to assess the error in mass values determined only from CO data and find these masses to be a factor of 2 lower than the masses based on ^{13}CO data. Thus, we determine the total molecular gas mass for the Cepheus bubble region to be $10^5\ M_\odot$. In Figure 5 we indicate the regions for which mass estimates are listed in Table 2. These boundaries are drawn only to identify what we interpret to be clouds, complexes of globules, or filamentary structures based on their continuity in the velocity channel maps.

We have used the H I 21 cm line data to compute the mass of the atomic gas associated with the Cepheus bubble. Without an a priori knowledge of the relevant range of velocities, it is difficult to distinguish the atomic gas associated with a given region that is close to the Galactic plane from the foreground and background material. We use our CO channel maps to select the velocity range of -27.5 to $+8.5$ km s^{-1}. The integrated emission in this velocity range is shown in Figure 6. This figure also compares the H I shell-like structure with the CO emission. An elongated cavity is seen in the H I map close to the inner northwest boundary of the bubble defined by the molecular emission. Closer to the Galactic plane, however, the H I emission gets stronger because of the inclusion of gas not associated with the bubble itself, and in this region an accurate comparison with CO emission becomes difficult. A detailed comparison of the clumpy and filamentary CO emission with the H I emission is not allowed by the poor angular resolution in the H I data. From these data, however, we estimate the atomic gas mass from the integrated intensity, assuming the line to be optically thin. We estimate the total atomic gas mass to be $3 \times 10^5\ M_\odot$. Within the uncertainties involved in the determination of both molecular and atomic masses, we can conclude that they are comparable, and that the total gas mass associated with the Cepheus bubble is approximately $4 \times 10^5\ M_\odot$.

3.4. *Energetics*

Figure 7 shows a plot of the LSR velocities in selected regions across the entire map. These regions were visually

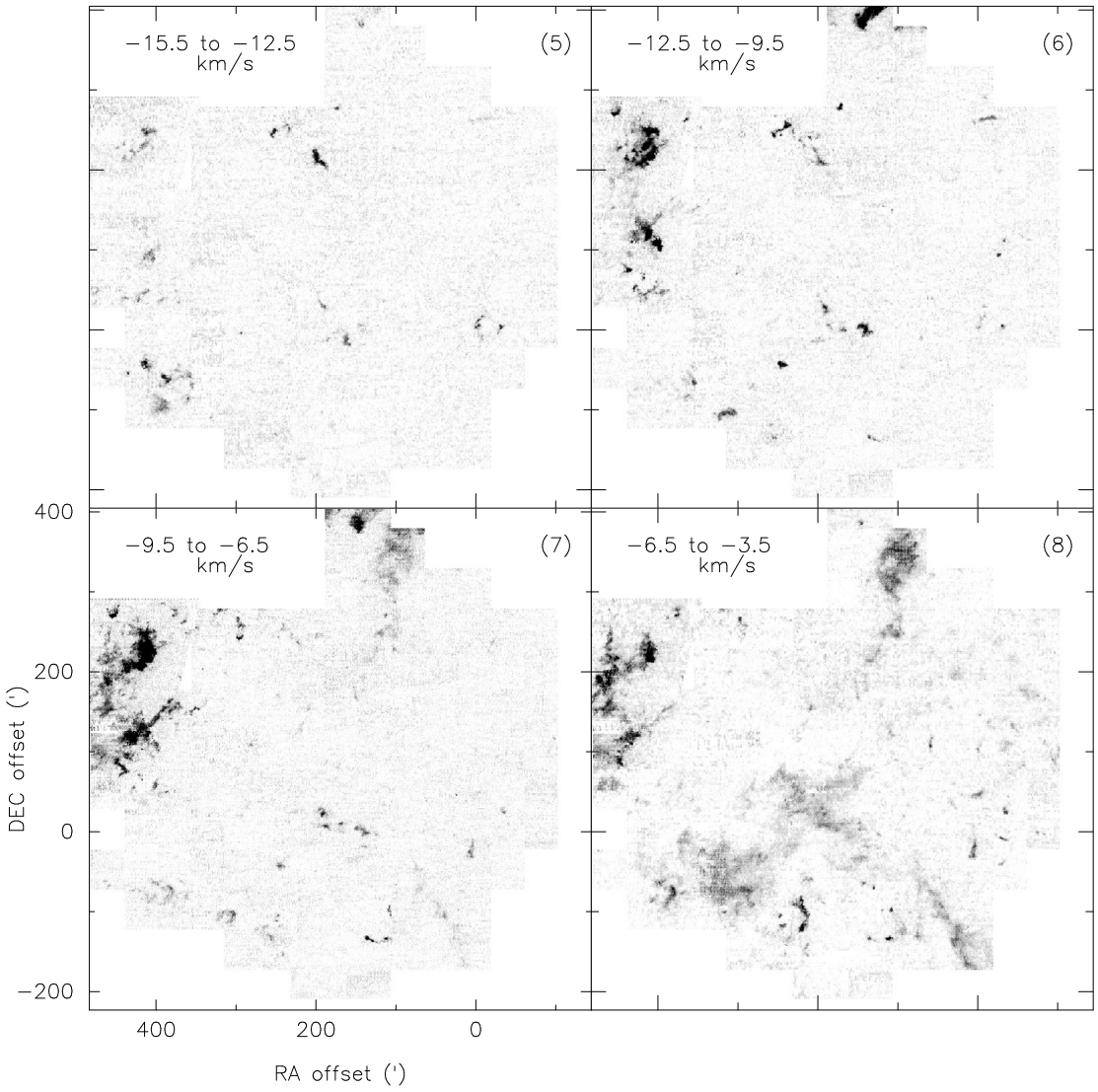

FIG. 2.—*Continued*

selected based on the peak intensity map. Each of the regions extends over a region typically several arcminutes in size and contains a few hundred spectra. We fitted Gaussians to the averaged spectrum of each of the 396 regions. The most negative velocity occurs in the southeastern corner of the region near S134 and the most positive velocity near the northwestern region near S133. The direction defined by these two regions is perpendicular to the Galactic plane with S133 away from the plane. This shear of ~ 13 km s^{-1} seen in Figures 2 and 7 is very unlikely to be due to a rotating ring as the binding mass required would be too large ($2 \times 10^6\ M_\odot$ for 13 km s^{-1} and radius of 60 pc; see panels 3 and 11 of Fig. 2). We interpret this bipolar feature of the velocity variation to represent expansion of an inhomogeneous, ellipsoidal bubble inclined with respect to our line of sight. Since the center of the bubble is well above the galactic plane, the expansion of the shell must proceed in an asymmetrical way (Silich et al. 1996). The kinetic energy in the system of molecular clouds associated with the Cepheus bubble is at least 10^{51} ergs obtained using the observed radial velocities with respect to the systemic velocity of $V_{\rm LSR} = -2$ km s^{-1}. There are deviations from this general expansion in several individual clouds, which may be because of acceleration attributable to the rocket effect as a consequence of the UV radiation from the stars belonging to the CepOB2 association.

If the shell was homogeneous and expanding uniformly, then one would expect the maximum red- and blueshifted emission to occur in the center and observe only transverse velocities at the periphery of the bubble. The observations indicate the highly red- and blueshifted emissions to occur at the rim of the shell. Based on the direction defined by the bipolar signature of the expansion, which is perpendicular to the Galactic plane, we interpret the large-scale kinematics to be the result of an expansion even though the overlap of red- and blueshifted emission, as seen in Figure 7, is only marginal. In our interpretation, the expanding shell is asymmetrical and is inclined with respect to our line of sight such that its expansion perpendicular to the Galactic plane produces the extreme Doppler-shifted components at the edges rather than at the center.

Another possibility is that the red- and blueshifted emission is due to an expansion caused by the second generation of stars. Such an expansion is, however, more likely to

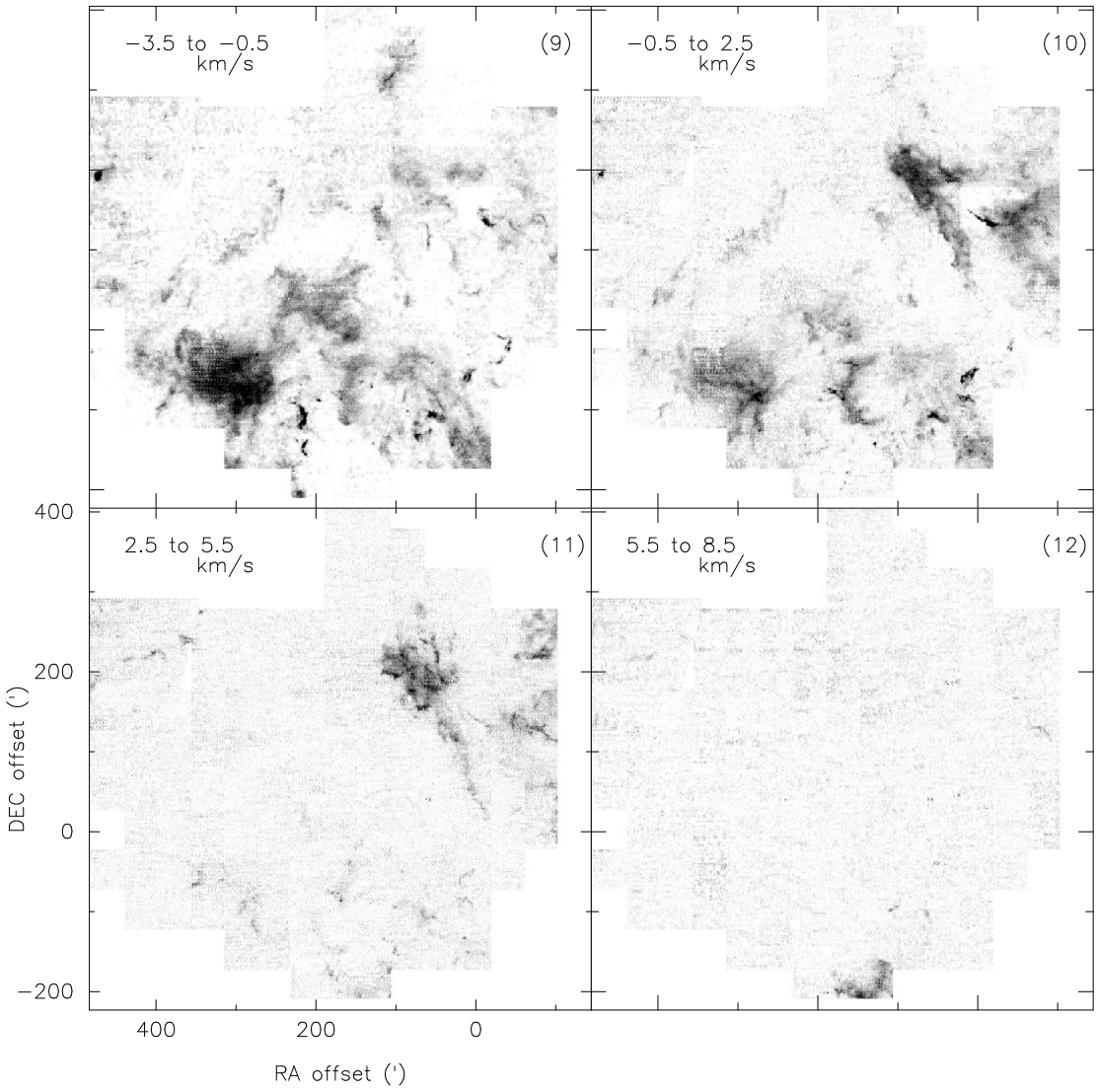

FIG. 2.—*Continued*

produce velocities that are tangential to the shell rather than radial, since these stars are expected to lie on the shell created by the first generation of stars. Such secondary expansion is characteristically relatively local, as is seen in the kinematics of the globules of IC 1396. The large-scale bipolar feature of red and blueshifted emission seen in Figure 7 is thus relatively unlikely to be due to a secondary expansion caused by the presently seen O- and B-type stars.

The shell is quite plausibly expanding anisotropically and has an elongated morphology as predicted by numerical models of expanding shells in the presence of a density gradient (see Fig. 2 of Silich et al. 1996). In § 4 and Figure 8 we consider a simple model in which we ignore the anisotropic expansion and asymmetrical morphology of the shell. We also assume the shell to be homogeneous. These drastic and clearly somewhat unrealistic simplifications are acceptable, however, inasmuch as our aim in this analysis is only to obtain rough estimates of the expansion timescale, size, and velocity of the shell.

4. DISCUSSION

4.1. *Origin of the Bubble*

Studies of large-scale expanding shells have been reviewed by Tenorio-Tagle & Bodenheimer (1988) and Bisnovatyi-Kogan & Silich (1995). Energy input from young massive stars with the processes of stellar winds, photoionization, and supernovae explosions adequately explain the sizes and energetics of galactic shells that have radii smaller than about 100 pc (McCray & Kafatos 1987).

Collisions of high-velocity clouds with the Galactic plane can give rise to large shells and form some high-z star-forming clouds such as the Orion-Monoceros complex (Tenorio-Tagle 1981; Franco et al. 1988). The shell-like structures created by this mechanism are very large compared with the size of the Cepheus bubble (about 120 pc).

The mass-loss rate for an O5-type star is $\sim 10^{-4}\ M_{\odot}$ yr^{-1}, and for an O9 star it is $\sim 10^{-8}\ M_{\odot}$ yr^{-1} (e.g., Lozinskaya 1992). The typical wind velocity of the outflowing matter is between 1000 and 3000 km s^{-1}. Thus the total energy input due to the stellar winds can be $\sim 10^{49}$–10^{51} ergs over a timescale of a few million years. This value of energy input is comparable with the observed total kinetic energy of the molecular clouds in the Cepheus bubble. However, this does not necessarily imply that stellar winds are the driving source of expansion. The stellar wind mechanism is more effective in a homogeneous medium,

TABLE 1

OB STARS BELONGING TO THE CEPOB2 ASSOCIATION

Number	PPM Number	HD Number	α(1950)	δ(1950)	$\Delta\alpha$ (arcmin)	$\Delta\delta$ (arcmin)	Spectral Type
1	22738	HD 239326	21 16 15.32	59:53:22.79	−13.13	23.38	B0
2	22763	HD 203374	21 17 54.17	61:38:46.60	−0.69	128.78	B0
3	22962	HD 205139	21 29 36.86	60:14:18.04	86.48	44.30	B0
4	23060	HD 206165	21 36 34.71	61:51:21.02	131.45	141.35	B2
5	23166	HD 207198	21 43 30.74	62:13:46.49	178.30	163.77	O9
6	23176	HD 207308	21 44 18.93	62:04:36.52	184.85	154.61	B2
7	23257	...	21 51 09.76	62:28:34.19	229.88	178.57	B1
8	23382	HD 209339	21 59 09.38	62:14:48.38	287.48	164.81	B0
9	23442	...	22 03 28.13	62:02:14.76	319.80	152.25	O5
10	23444	HD 209975	22 03 36.25	62:02:10.90	320.76	152.18	O5
11	23640	HD 211880	22 16 50.91	62:58:18.62	401.14	208.31	B2
12	23731	HD 213023	22 25 12.25	63:27:46.03	450.38	237.77	B2
13	39180	HD 239581	21 07 01.45	55:50:31.46	−92.44	−219.48	B
14	39225	HD 202214	21 10 31.84	59:46:48.94	−56.39	16.82	B2
15	39278	HD 239618	21 13 27.36	59:33:08.83	−34.54	3.15	B0
16	39477	...	21 25 41.45	55:59:24.79	64.53	−210.59	B0
17	39480	HD 239676	21 26 08.26	59:04:34.56	62.73	−25.42	B2
18	39498	...	21 27 31.42	58:31:12.91	74.60	−58.78	O9
19	39533	...	21 29 15.06	56:58:45.00	91.97	−151.25	B2
20	39557	...	21 30 07.93	57:16:51.83	98.36	−133.14	B0
21	39627	...	21 34 11.76	57:14:34.86	131.45	−135.42	B0
22	39653	...	21 35 28.74	57:54:53.09	139.27	−95.12	B2
23	39704	...	21 37 24.45	57:15:44.20	157.43	−134.26	O6
24	39766	...	21 40 50.18	57:30:25.14	184.01	−119.58	B0
25	39790	HD 239748	21 42 08.06	58:00:34.87	191.79	−89.42	B2
26	39815	...	21 43 02.44	58:49:35.27	194.43	−40.41	B0
27	39816	...	21 43 00.30	57:13:21.64	203.06	−136.64	B2
28	39848	...	21 44 35.85	57:33:39.33	214.00	−116.34	B2
29	39853	...	21 44 45.37	56:41:07.14	220.43	−168.88	B0
30	39875	...	21 46 08.49	59:28:03.40	214.45	−1.94	B0
31	39955	HD 239789	21 51 28.41	58:07:26.63	265.15	−82.56	B2
32	40131	HD 239828	21 59 42.56	59:15:38.05	319.79	−14.37	B2
33	40148	HD 209481	22 00 23.53	57:45:31.01	339.24	−104.48	O9
34	40305	...	22 08 36.07	57:53:38.39	403.41	−96.36	B
35	40324	HD 210839	22 09 48.54	59:10:01.75	398.31	−19.97	O4
36	40345	...	22 10 47.01	57:01:05.21	431.01	−148.91	B0
37	40368	HD 239895	22 11 30.68	57:25:04.62	432.24	−124.92	B2
38	40500	HD 239923	22 17 34.60	58:42:05.99	464.25	−47.90	B2
39	...	HD 204150	21 22 55.32	60:34:52.70	36.26	64.88	B2
40	...	...	21 35 15.66	57:21:31.30	139.65	−128.48	B2
41	...	HD 206327	21 37 38.43	61:19:45.50	141.35	109.76	B2
42	...	HD 207017	21 42 24.11	62:32:28.70	168.78	182.48	B2
43	...	HD 207951	21 49 13.56	61:34:06.40	223.00	124.11	B2
44	...	HD 208266	21 51 29.06	60:24:22.20	248.04	54.37	B1
45	...	...	21 52 21.84	62:22:40.50	238.99	172.67	B1
46	...	...	21 52 26.90	62:21:48.30	239.69	171.80	B1
47	...	HD 208905	21 55 46.15	61:03:23.00	274.18	93.38	B1
48	...	HD 209454	21 59 53.02	61:18:52.50	301.56	108.87	B2
49	...	...	21 37 06.13	57:08:26.30	155.47	−141.56	B1
50	...	...	21 37 53.96	57:15:23.40	161.45	−134.61	B0
51	...	HD 239743	21 41 18.87	60:03:59.60	174.51	33.99	B2

NOTE.—Units of right ascension are hours, minutes, and seconds, and units of declination are degrees, arcminutes, and arcseconds.

whereas the gas surrounding the OB stars already has been largely evacuated by the photoionization effects that start as soon as the OB stars turn on. It is likely that the clearing out of matter around these stars took place early in the history of this region because of the photoionizing UV radiation. Specifically, the rocket effect (Oort & Spitzer 1955; Elmegreen 1976; McKee, van Buren, & Lazareff 1984; Bertoldi & McKee 1990; Patel et al. 1995) is a powerful acceleration mechanism. This acceleration mechanism does not require a homogeneous shell; in fact, a clumpy medium allows a more effective penetration of the UV radiation and allows clumps or globules deeper within the clumpy molecular cloud to undergo rocket acceleration as seen, for example, in some of the globules associated with the Rosette molecular cloud (Patel, Xie, & Goldsmith 1993).

The size scales and timescales for the production of such cavities around OB stars have been discussed by Elmegreen (1976) and McKee et al. (1984). In terms of the initial gas density n (cm^{-3}), the radius of such a cavity around an O4–O9 star reaches $\sim 56 n^{-0.3}$ pc and velocity $\sim 6.8(S_{48}/n)^{1/4}$ km s^{-1} over the main-sequence lifetime of the O stars, which is given by $2.5 \times 10^6 S_{48}^{-1/4}$ yr^{-1} (McKee et al. 1984). S_{48} is the flux of ionizing photons in units of 10^{48} s^{-1}.

The supernova rate in a typical OB association is approximately one per 10^5–3×10^5 yr (Lozinskaya 1992; McCray

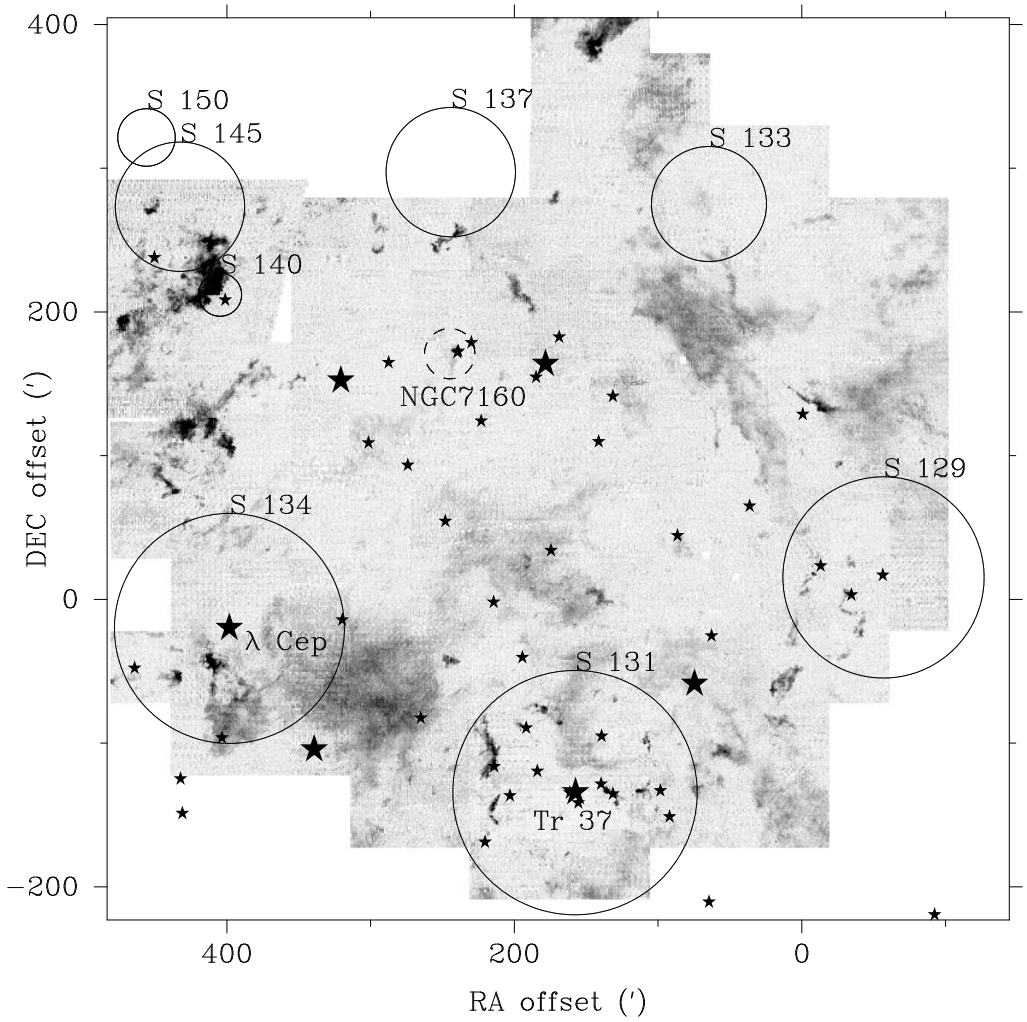

FIG. 3.—Sharpless H II regions and the CepOB2 association. The locations of the H II regions from the Sharpless catalog are indicated by circles, which have radii representing the approximate angular extent of the H II region. Except IC 1396 (S131), the H II regions do not have circular morphologies. The larger star symbols indicate O-type stars and smaller star symbols indicate stars of spectral types B0–B2.

& Kafatos 1987). We find the dynamical age of the IC 1396 region to be about 3 Myr (Patel et al. 1995). Over a timescale of a few million years, we can reasonably assume, therefore, that at least one supernova explosion has occurred in the Cepheus bubble region. There is no detection of a supernova remnant in either the radio surveys or the X-ray survey by Einstein or *ROSAT*, but this could be due to the relatively large age of the supernova. The detected remnants are typically less than a million years old (Ilovaisky & Lequeux 1972). The existence of the runaway star, λ Cephei, suggests that its binary companion could have exploded as a supernova somewhere in the central region of the Cepheus bubble (Kun et al. 1987). Another runaway star, 68 Cygni, is also likely to have originated in the CepOB2 region (Blaauw 1961). The proper motion of the runaway star λ Cep of ~ 70 km s^{-1} (toward the direction of southeast), when projected back to the center of the Cepheus bubble, indicates a kinematic age of $\sim 3 \times 10^6$ yr (Kun et al. 1987). According to Blaauw (1964), this star may have been a companion to a more massive supernova progenitor in the central region of the Cepheus bubble. This relatively small value of the kinematic age is inconsistent with the age of NGC 7160 (10–18 Myr; see § 3.1), but this could be simply explained if the supernova event associated with λ Cep is only the most recent of a number of such events in the history of the Cepheus bubble. The least massive star that is expected to end its life as a Type II supernova has an initial mass of $\sim 7\ M_\odot$ (Trimble 1982). The lifetime of such a star is $\sim 5 \times 10^7$ yr (McCray & Kafatos 1987). Thus, the mean supernova rate in a typical OB association that contains about 20–40 B3-type stars is one every $\lesssim 10^6$ yr. A quite distinct argument supporting the idea that one or more supernovae occurred in this region concerns the properties of dust in and around IC 1396, which suggests that it has been preheated by shocks presumably due to supernovae (Clayton & Fitzpatrick 1987).

4.2. *Triggered Star Formation*

The idea of triggered star formation goes back several decades (Bok & Reily 1947; Opik 1953; Oort 1954; Dibai 1958). In the Cepheus bubble region, the presence of OB stars and young stellar objects represented by *IRAS* sources arranged in a circular pattern suggests that the parent gas has been either compressed by external pressure originating at the center of the bubble produced by the previous generation of massive stars, or that the gas has been relocated (without an enhancement of the star formation efficiency)

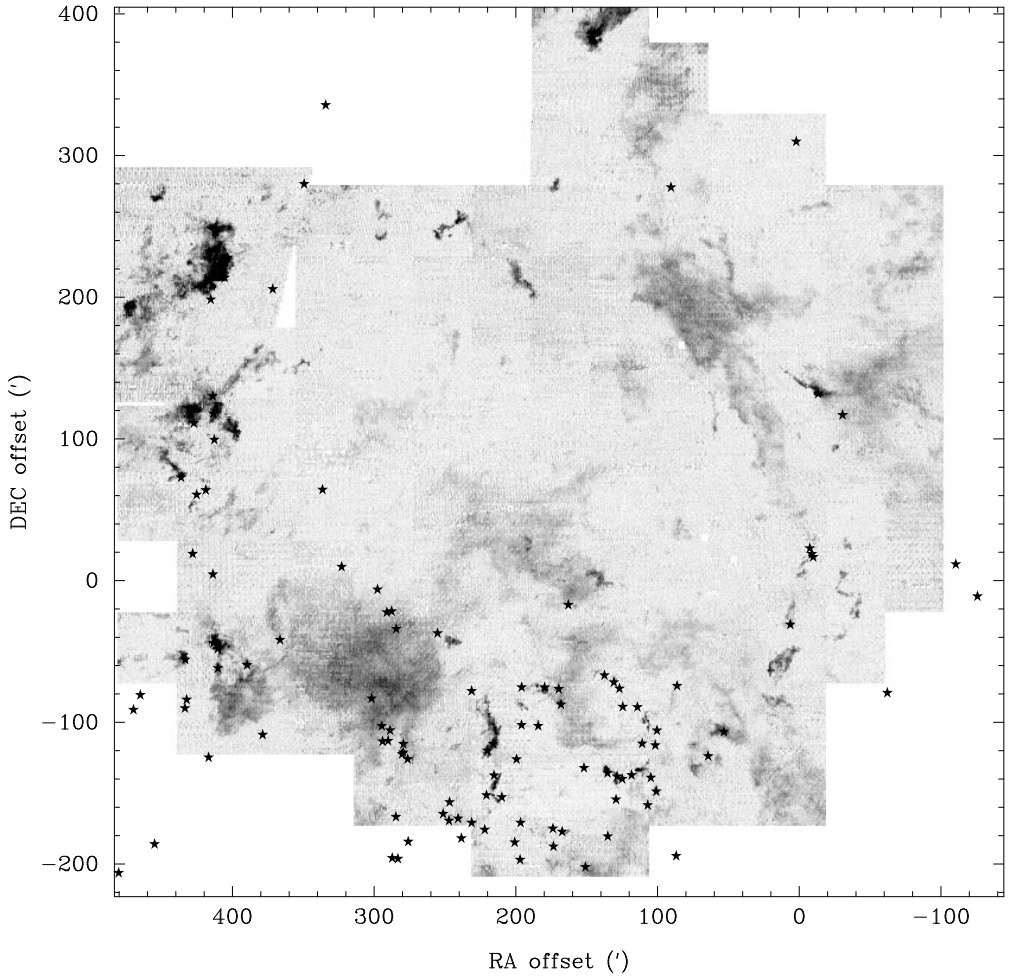

FIG. 4.—*IRAS* point sources in the field of the Cepheus bubble. The sources were selected according to color criteria that emphasize young stellar objects. Note that several sources appear coincident with the globules and filamentary structures seen on the CO map. The diffuse clouds lack *IRAS* sources.

by such forces. The latter case is an example of "weak triggering" (Elmegreen 1992). The *IRAS* sources embedded in the heads of cometary globules, as seen for example in IC 1396, suggest strong triggering where star formation has occurred much more rapidly than would have been the case without the photoionization-induced collapse (Bertoldi & McKee 1990 and references therein).

Gravitational instabilities in expanding shells have been studied analytically by Vishniac (1983), Elmegreen (1989, 1992), Comerón & Torra (1994), and McCray & Kafatos (1987). We estimate the timescale for this instability as well as the size, velocity of expansion, and the collected mass of the shell at which the instability occurs by solving numerically the equation of motion of the shell following Mazurek (1980) and Maddalena & Morris (1980). If M_s denotes the mass of the shell and U_s its velocity, then momentum conservation condition gives

$$\frac{d}{dt}(M_s U_s) = 4\pi r^2 P - \frac{GM_s(M_s + 2M_{\rm II})}{2r^2} - U_{\rm II}\frac{d}{dt}M_{\rm II}\,, \quad (1)$$

where P is the pressure in the interior of the shell (in the H II region), $M_{\rm II}$ is the ionized gas mass, r is the radius of the shell and $U_{\rm II} = U_s/2$ is the velocity of the ionized gas.

We solved equation (1) numerically with initial conditions corresponding to the Stromgren sphere values of radius, velocity, and enclosed ionized gas mass. Assuming the gas temperature within the H II region to be 7500 K, we find that the isothermal speed of sound in the H II region is 11.2 km s^{-1}, and that the initial shell expansion velocity is 12.9 km s^{-1}. The Stromgren radius is given by $r_0^3 = 3L/4\pi\alpha n_c^2$, where L is the ionizing photon luminosity, α is the hydrogen recombination coefficient, and n_c is the initial cloud proton density, $n_c = 2n_{\rm H_2}$.

The variables in equation (1) are transformed to dimensionless quantities $x = r/r_0$ and $y = U_s^2/C^2$, where C is the speed of sound in the ionized gas. Then it follows that the expansion of the shell is described by a first order differential equation of y with x as the independent variable (Mazurek 1980). According to the Elmegreen & Lada (1977) mechanism, as the thin shell expands and grows in mass, but at a certain critical column density $\sigma = 2.14(p_{\rm II}/\pi G)^{1/2}$, the shell becomes gravitationally unstable, which leads to the gravitational collapse within the shell. In the above equation, $p_{\rm II}$ is the pressure within the shell. The instability occurs when $x = x_c$, where x_c is given by (Mazurek 1980)

$$x_c = 21.3\left(\frac{L}{10^{49}\ \mathrm{s}^{-1}}\right)^{4/21}\left(\frac{n_c}{10^3\ \mathrm{cm}^{-3}}\right)^{4/42}\left(\frac{T}{10^4\ \mathrm{K}}\right)^{4/14}. \quad (2)$$

The initial conditions depend upon two parameters, $n_{\rm H_2}$ and L, the molecular hydrogen density of the initial cloud and the UV photon luminosity of the young massive star(s)

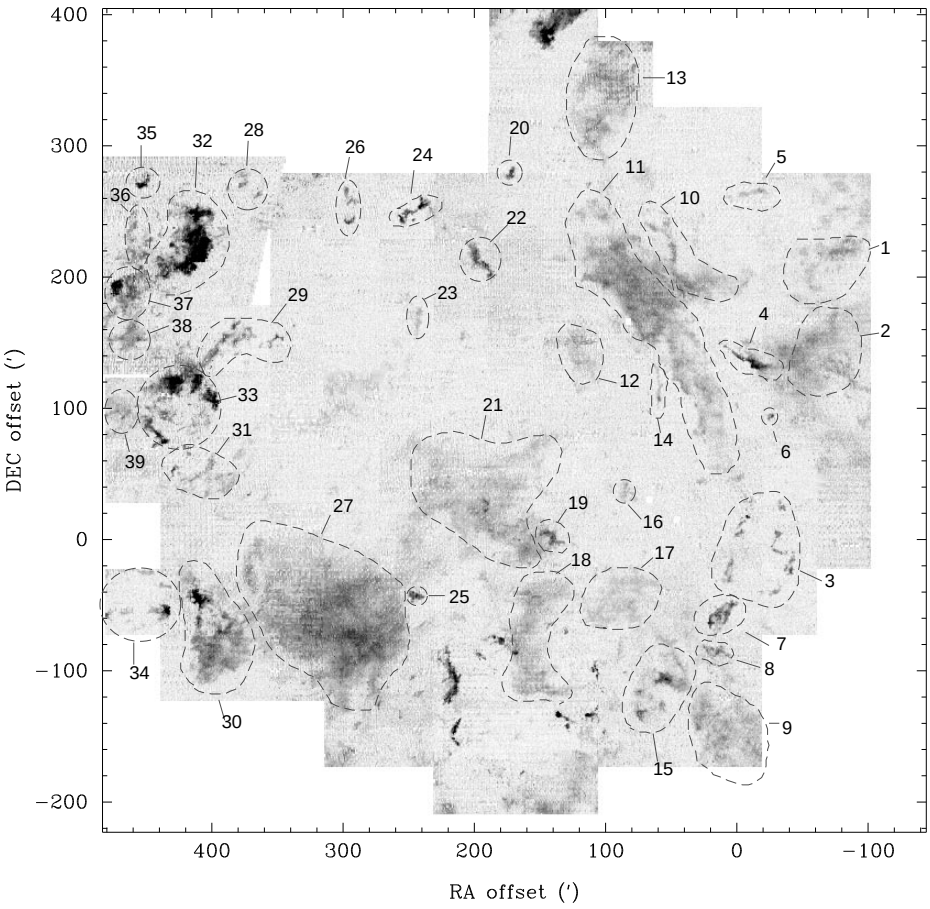

FIG. 5.—Approximate outlines of the regions over which mass estimates were obtained from the CO data. The numbers refer to the entries in Table 2. Most of the globules, filaments, and diffuse clouds shown in this figure have not been previously identified. Exceptions are noted in the last column of Table 2. The IC 1396 region is not labeled in this figure and the corresponding mass values are absent in Table 2, as these have been published elsewhere (Patel et al. 1995). The total mass of the molecular gas in IC 1396 is 2200 $M_{\odot}$.

creating the H II region. We solved equation (1) for 1 cm^{-3} $\leq n_{H_2} \leq$ 500 cm^{-3} and 10^{47} s^{-1} $\leq L \leq 5.0 \times 10^{48}$ s^{-1}, stopping the time evolution when $x = x_c$ or $u_s = 0$. We find that $n_{H_2} = 10$ cm^{-3} and $L = 8.0 \times 10^{47}$ s^{-1} for a shell to become unstable on reaching a radius of about 30 pc, which is roughly the radius of the ring defined by the O-type stars in Figure 3. The instability occurs at an age of about 7 Myr, and the mass accumulated by such a shell is about 6.0×10^4 $M_{\odot}$. This mass value is in good agreement with the observed mass of the Cepheus bubble.

4.3. *Evolution of the Cepheus Bubble*

We propose that the evolution of the Cepheus bubble region has proceeded in the following manner. The bubble originated from a compressed shell of gas that was blown out by the combined effects of stellar winds and photoionization from OB stars of the first generation. These stars are no longer present, as they have already exploded as supernovae. We interpret the old cluster NGC 7160 and the evolved stars such as μ Cephei, VV Cephei, and ν Cephei to be some of the companions of the first generation of OB stars.

The expanding shell around the first generation of OB stars is shown schematically in Figure 8*a*. We showed in § 4.2 that such a shell will become unstable after a period of ~7 Myr after the birth of the progenitor OB stars. The calculated radius of such a shell (30 pc) at the time of the instability is also consistent with the radius of the ring of O and B-type stars belonging to CepOB2. The age of NGC 7160 is 13–18 Myr (see § 3.1) and the age of CepOB2 is ~7 Myr (Marshall, Comins, & Karschner 1990). Thus the instability timescale of 7 Myr is consistent with the idea of CepOB2 having formed due to such an instability. Figures 8*b* and 8*c* show this stage of the evolution of the Cepheus bubble.

Once the OB association CepOB2 is formed, it immediately starts to affect the dense gas remaining from the parent shell. This gas around the O-type stars expands in the form of rings as seen in the cases of IC 1396 and L1204 because of secondary expansion (Fig. 8*c*). The dynamical timescale of these expanding subsystems is between 1 and 3 Myr, which is roughly consistent with the age of CepOB2. The sound crossing time in the globules such as those seen in IC 1396, is less than a million years. Therefore, the globules have sufficient time to have undergone radiative implosion while they are moving away from the O stars. The *IRAS* point sources associated with the globules represent the third generation of stars currently forming in the region of the Cepheus bubble (Fig. 8*d*).

The present molecular material then represents surviving fragments of clouds that evolved from the original shell depicted in Figures 8*a* and 8*b* and that are now being eroded further and accelerated because of the photoionization by the O stars of CepOB2. Based on the masses of the

TABLE 2

MASS ESTIMATES

Number	α(1950)	δ(1950)	Mass ($M_\odot$)	Association
1.....	21 05	63 14	660	...
2.....	21 10	61 44	5000	...
3.....	21 15	59 00	600	S129
4.....	21 15	61 53	700	...
5.....	21 16	63 55	100	...
6.....	21 14	61 02	60	...
7.....	21 19	58 28	720	...
8.....	21 20	58 05	320	...
9.....	21 21	57 16	3900	...
10	21 25	63 18	1540	S133
11	21 30	62 30	11400	...
12	21 35	62 00	300	...
13	21 35	64 40	4400	NGC 7129
14	21 26	61 28	100	...
15	21 25	57 30	2240	...
16	21 29	60 08	100	...
17	21 30	58 33	1600	L1116
18	21 38	58 26	3700	...
19	21 35	59 27	60	L1131
20	21 44	64 09	120	...
21	21 45	60 00	8540	L1144
22	21 47	63 08	700	NGC 7139
23	21 52	62 18	100	...
24	21 55	63 36	440	S137
25	21 49	58 48	320	...
26	22 02	63 33	240	...
27	21 54	58 24	25200	L1149, L1143
28	22 15	64 08	200	...
29	22 10	62 00	520	...
30	22 10	58 30	6660	S134
31	22 10	60 11	720	...
32	22 20	63 37	8040	S 140
33	22 13	61 18	3900	L 1204
34	22 19	58 33	460	...
35	22 27	64 04	380	...
36	22 27	63 25	600	...
37	22 25	62 29	2720	L 1203
38	22 23	62 06	1480	...
39	22 22	61 05	300	...

NOTE.—Units of right ascension are hours and minutes and units of declination are degrees and arcminutes.

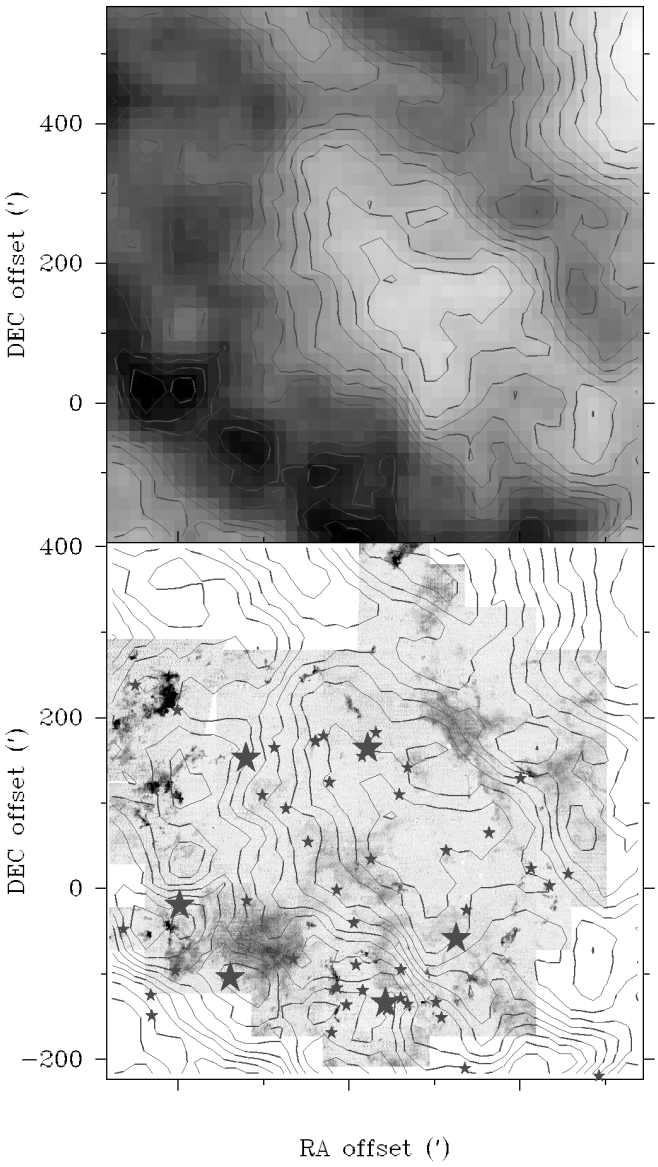

FIG. 6.—21 cm H I line emission from the Cepheus bubble. *Top panel*: the gray scale and contour representation of the integrated intensity of the 21 cm line from the neutral atomic hydrogen mapped with an angular resolution of about 30′. The velocity range of the integrated emission is between −27.5 and 8.5 km s^{-1}, which corresponds to the range of velocities covered by the CO emission. The contour levels are 50, 100, 200, 300... 1200 K km s^{-1}. *Bottom panel*: the H I emission (the same contour levels as above) overlaid on the CO emission and OB stars. The cavity in H I emission is roughly consistent with the interior of the Cepheus bubble as defined by the CO clouds.

globules such as those seen in IC 1396, and the UV flux incident upon them, one can show that these globules have an evaporation time of 10^7 yr. The future of the Cepheus bubble thus depends on dense molecular clouds in the form of globules and filaments that subsequently get blasted by supernovae explosions occurring once every 10^5–10^6 yr over the next several million years. There will be no further generation of high-mass stars within the Cepheus bubble and hence relatively little propagation of star formation, as the stars currently forming in the surviving globules have low to intermediate masses.

5. CONCLUSIONS

The Cepheus bubble region provides a test bench for studying the phenomena associated with the interaction of massive stars and the interstellar medium, and specifically, the process of propagating star formation by sequential triggering. Our CO map of this region reveals the molecular clouds associated with the bubble to exhibit a signature of an asymmetrical expansion away from the Galactic plane as is expected on the basis of recent models of expanding shells with their origins displaced from the Galactic plane. Based on the CO and H I data, we estimate the total molecular gas mass to be $1 \times 10^5\ M_\odot$ and the atomic gas mass to be 3 times this value, with the total gas mass thus equal to $4 \times 10^5\ M_\odot$. The formation of the CepOB2 association lying within the molecular Cepheus bubble is consistent with the idea of triggered star formation due to compression of a thin shell around the previous generation of massive stars, the companions of which are presently seen as members of NGC 7160. *IRAS* point sources in the globules and molecular clouds associated with the Cepheus bubble suggest that a third generation of low- to intermediate-mass stars has recently formed and/or is currently forming in these clouds.

Better age estimates based on optical observations of the stars in this region will be useful to corroborate the evidence

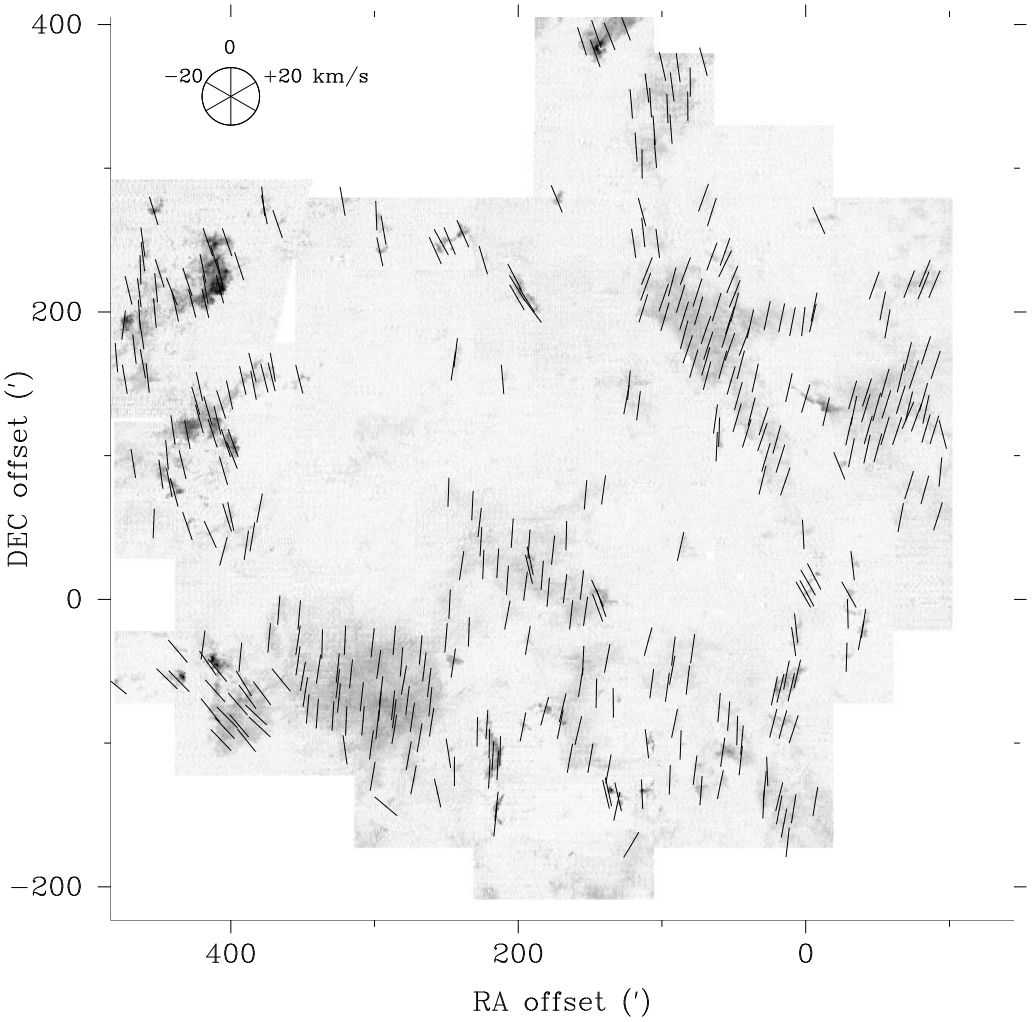

FIG. 7.—Centroid LSR velocities of the CO spectra averaged over selected regions are shown in this vector plot. The direction of each segment indicates the velocity as shown in the key located in the upper left corner. The LSR velocities as shown in the channel maps of Fig. 2 have been offset by -2 km s^{-1}, which is the velocity of the ionized gas, taken to be the mean velocity of the clouds in this region. The correction due to differential Galactic rotation is less than 0.5 km s^{-1} across the map and is neglected.

for sequentially triggered star formation. Proper motion study of the stars in CepOB2 association using the data from *Hipparcos* mission will also be very useful in understanding their kinematic origins. Finally, the CO data presented here will hopefully lead to further millimeter and submillimeter mapping of the clouds to understand their detailed physical and chemical state and their kinematic structure and also to understand better the influence of UV radiation and supernova shocks on these objects.

We gratefully acknowledge the help and support from the staff of the FCRAO during observations at Quabbin. We are grateful to G. Moriarty-Schieven for the 21 cm spectral line data from DRAO. This work has made use of the SIMBAD database, operated at CDS, Strasbourg, France.

REFERENCES

Ábráham, P., Kun, M., Balázs, L. G., Holl, A., & Fronto, A. 1993, A&A, 268, 230
Beichman, C. A., Boulanger, F., & Moshir, M. 1992, ApJ, 386, 248
Bertoldi, F., & McKee, C. 1990, ApJ, 354, 529
Bisnovatyi-Kogan, G. S., & Silich, S. A. 1995, Rev. Mod. Phys., 67, 661
Blaauw, A. 1961, Bull. Astron. Inst. Netherlands, 15, 265
———. 1964, ARA&A, 2, 213
Bok, B. J., & Reily, E. F. 1947, ApJ, 105, 255
Carpenter, J., Snell, R., & Schloerb, F. P. 1995, ApJ, 445, 246
Clayton, G. C., & Fitzpatrick, E. L. 1987, AJ, 93, 157
Comerón, F., & Torra, J. 1994, ApJ, 423, 652
Conti, P. S., & van den Huevel, E. P. J. 1970, A&A, 9, 499
Cruz-Gonzalez et al. 1974, Rev. Mexicana Astron. Astrofis., 1, 211
Dame, T. M., Ungerechts, H., Cohen, R. S., De Geus, E. J., Grenier, I. A., May, J., Murphy, J. C., Nyman, L. A., & Thaddeus, P. 1987, ApJ, 322, 706
Dibai, E. A. 1958, Soviet Astron., 2, 429
Dobashi, K., Bernard, J., Yonekura, Y., & Fukui, Y. 1994, ApJS, 95, 419
Dubout-Crillon, R. 1976, A&AS, 25, 25
Elmegreen, B. G. 1976, ApJ, 205, 405
———. 1989, ApJ, 344, 306
———. 1992, in Third Canary Islands Winter School of Astrophys., Star Formation in Stellar Systems, ed. F. Sanchez, M. Prieto, & G. Tenorio-Tagle (Cambridge: Cambridge Univ. Press), 381
Elmegreen, B. G., & Lada, C. J. 1977, ApJ, 214, 725
Erickson, N. R., Goldsmith, P. F., Novak, G., Grosslein, R. M., Viscuso, P. J., Erickson, R. B., & Predmore, C. R. 1992, IEEE Trans. Microwave Theory and Techniques, 40, 1
Franco, J., Tenorio-Tagle, G., Bodenheimer, P., Rozyczka, M., & Mirabel, I. F. 1988, ApJ, 333, 826
Garmany, C. D., Conti, P. S., & Chiosi, C. 1982, ApJ, 263, 777
Gies, D. R. 1987, ApJS, 64, 545

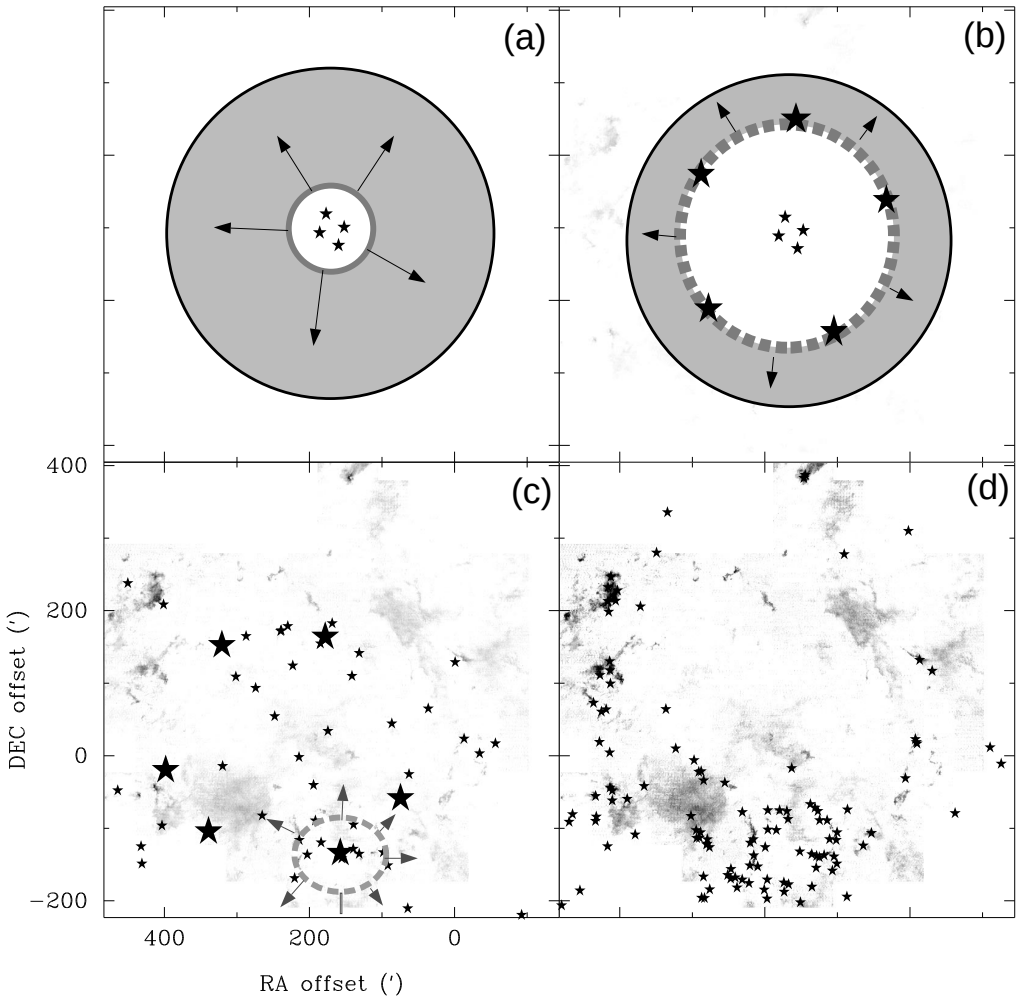

FIG. 8.—Time evolution of the Cepheus bubble. *a*: A cluster of high-mass stars forms in a parent molecular cloud, giving rise to a Stromgren sphere surrounded by a thin expanding shell that collects mass as it expands. *b*: Gravitational instability leads to fragmentation of this shell after a period of ~7 Myr, leading to formation of OB stars (CepOB2) shown in *c*. Secondary expansion of material around these stars (grey dotted line in panel *c*), is in the form of a ring (e.g., IC 1396). Panel *d* is a reproduction of Fig. 4 showing the *IRAS* point sources representing the third generation of low- to intermediate-mass stars recently formed in the compressed regions.

Heyer, M. H., Brunt, C., Snell, R. L., Howe, J. E., Schloerb, F. P., & Carpenter, J. M. 1997, ApJS, 115, 241
Heyer, M. H., Carpenter, J. M., & Ladd, E. F. 1996, ApJ, 463, 630
Humphreys, R. M. 1978, ApJS, 38, 309
Ilovaisky, S. A., & Lequeux, J. 1972, A&A, 20, 347
Janes, K., & Adler, D. 1982, ApJS, 49, 425
Karimova, D. K., & Pavlovskaya, E. D. 1981, Soviet Astron. Lett., 7, 347
Keto, E., & Ho, P. T. P. 1989, ApJ, 347, 349
Kun, M., Balázs, L. G., & Toth, I. 1987, Ap&SS, 134, 211
Leisawitz, D., Bash, F. N., & Thaddeus, P. 1989, ApJS, 70, 731
Lozinskaya, T. 1992, Supernovae and Stellar Wind in the Interstellar Medium (New York: AIP)
Maddalena, R., & Morris, M. 1980, ApJ, 323, 179
Marshall, L. A., Comins, N. F., & Karschner, G. B. 1990, AJ, 99, 1536
Mazurek, T. J. 1980, A&A, 90, 65
McCray, R., & Kafatos, M. 1987, ApJ, 317, 190
McKee, C. F., van Buren, D., & Lazareff, B. 1984, ApJ, 278, L115
Oort, J. H. 1954, Bull. Astron. Inst. Netherlands, 12, 177
Oort, J. H., & Spitzer, L. 1955, ApJ, 121, 6
Opik, E. J. 1953, Irish. Astron. J., 145, 811
Patel, N. A., Goldsmith, P. F., Snell, R. L., Hezel, T., & Xie, T. 1995, ApJ, 447, 721
Patel, N. A., Xie, T., & Goldsmith, P. F. 1993, ApJ, 413, 593
Pedlar, A. 1980, MNRAS, 192, 179
Roeser, S., & Bastian, U. 1988, A&AS, 74, 449
Rolfs, K., & Wilson, T. L. 1996, Tools of Radio Astronomy (Heidelberg: Springer), 390
Sharpless, S. 1959, ApJS, 4, 257
Silich, S. A., Franco, J., Palous, J., & Tenorio-Tagle, G. 1996, ApJ, 468, 722
Simonson, C. S., III, & van Someren Greve H. W. 1976, A&A, 49, 343
Simonson, S. C. 1968, ApJ, 154, 923
Sivan, J. P. 1974, A&AS, 16, 163
Sridharan, T. K. 1992, J. Astrophys. Astron., 13, 217
Stone, R. 1979, ApJ, 232, 520
Tenorio-Tagle, G. 1981, A&A, 94, 338
Tenorio-Tagle, G., & Bodenheimer, P. 1988, ARA&A, 26, 145
Trimble, V. 1982, Rev. Mod. Phys., 54, 1183
Vishniac, E. T. 1983, ApJ, 274, 152
Xie, T., & Goldsmith, P. F. 1994, ApJ, 430, 252